Journal of Solid State Chemistry 184 (2011) 365–372

Contents lists available at ScienceDirect

Journal of Solid State Chemistry

journal homepage: www.elsevier.com/locate/jssc

# Mixed conductivity, structural and microstructural characterization of titania-doped yttria tetragonal zirconia polycrystalline/titania-doped yttria stabilized zirconia composite anode matrices

M.T. Colomer [a,*], M. Maczka [b]

[a] Instituto de Cerámica y Vidrio, CSIC, c/Kelsen no 5, 28049 Madrid, Spain
[b] Institute of Low Temperature and Structure Research, Polish Academy of Sciences, P.O. Box 1410, Wroclaw 2, Poland

ARTICLE INFO

*Article history:*
Received 19 October 2010
Received in revised form
1 December 2010
Accepted 3 December 2010
Available online 8 December 2010

*Keywords:*
Ti-doped YSZ
Ti-doped YTZP
$ZrTiO_4$
Zirconium titanate
$Y_2(Ti,Zr)_2O_7$
Pyrochlore
SOFC

ABSTRACT

Taking advantage of the fact that $TiO_2$ additions to 8YSZ cause not only the formation of a titania-doped YSZ solid solution but also a titania-doped YTZP solid solution, composite materials based on both solutions were prepared by solid state reaction. In particular, additions of 15 mol% of $TiO_2$ give rise to composite materials constituted by 0.51 mol fraction titania-doped yttria tetragonal zirconia polycrystalline and 0.49 mol fraction titania-doped yttria stabilized zirconia (0.51TiYTZP/0.49TiYSZ). Furthermore, $Y_2(Ti_{1-y}Zr_y)_2O_7$ pyrochlore is present as an impurity phase with $y$ close to 1, according to FT-Raman results. Lower and higher additions of titania than that of 15 mol%, i.e., $x=0, 5, 10, 20, 25$ and 30 mol% were considered to study the evolution of 8YSZ phase as a function of the $TiO_2$ content. Furthermore, zirconium titanate phase ($ZrTiO_4$) is detected when the titania content is equal or higher than 20 mol% and this phase admits $Y_2O_3$ in solid solution according to FE-SEM-EDX.

The 0.51TiYTZP/0.49TiYSZ duplex material was selected in this study to establish the mechanism of its electronic conduction under low oxygen partial pressures. In the $pO_2$ range from 0.21 to $10^{-7.5}$ atm. the conductivity is predominantly ionic and constant over the range and its value is 0.01 S/cm. The ionic plus electronic conductivity is 0.02 S/cm at 1000 °C and $10^{-12.3}$ atm. Furthermore, the onset of electronic conductivity under reducing conditions exhibits a $-1/4$ $pO_2$ dependence. Therefore, it is concluded that the n-type electronic conduction in the duplex material can be due to a small polaron-hopping between $Ti^{3+}$ and $Ti^{4+}$.



## 1. Introduction

Mixed conductors should be able to replace the state of the art of solid oxide fuel cell (SOFC) anode cermets. In mixed conductors both ionic and electronic defects are present in non-negligible concentrations and their mobility is so significant that the electrode reaction can proceed at any point of the electrode surface. The usual requirement of a triple phase contact where electrode, electrolyte and gas phase are in contact, is replaced by a simple requirement of a two phase boundary region between electrode (mixed conductor) and gas phase. In this manner it is expected that polarization losses associated with the SOFC anode process can be minimized [1]. Mixed conductors based on yttria stabilized zirconia (YSZ) or yttria-tetragonal zirconia polycrystalline (YTZP) are usually obtained if a significant amount of a mixed valence dopant cation is introduced in solid solution. In the last two decades research efforts have been concentrated mainly on the titania-doped yttria-stabilized zirconia and on the titania-doped yttria tetragonal zirconia solid solution mixed conductors as matrices for anode cermets [2–12]. Although both solid solutions have been separately studied, the same cannot be said with respect to the composite materials based on both systems. Only the study of tetragonal/cubic zirconia composite electrolytes has been recently carried out [13]. In comparison to YSZ (8 mol% $Y_2O_3$), the YTZP (3 mol% $Y_2O_3$) is also an oxygen ion conductor and below 700 °C its conductivity was found to be higher than that of YSZ cubic solid solution [14]. In addition, YTZP material has shown to be a tougher material [15]. These two combined characteristics make Ti-doped YSZ/Ti-doped YTZP composite materials attractive for application in electrochemical devices, but many aspects of these materials are still unknown. Although isothermal sections [7,16,17] for the $ZrO_2$–$Y_2O_3$–$TiO_2$ ternary system have been reported, it must be taking into account that the phase diagrams are outlined based on the results obtained for samples sintered at 1500 °C for at least 36 h whereas in the present study the sintering time was only of 2 h. For this reason, the phases obtained during the present investigations may be different from those obtained with longer sintering times. The purpose of this study is to follow the 8YSZ phase evolution after the addition of $TiO_2$. This work is also focused

* Corresponding author.
*E-mail address:* tcolomer@icv.csic.es (M.T. Colomer).

0022-4596/$ - see front matter © 2010 Elsevier Inc. All rights reserved.
doi:10.1016/j.jssc.2010.12.006

on the structural, microstructural and electrical characterization of a Ti-doped YTZP/Ti-doped YSZ duplex material that could be used as matrix in a SOFC anode.

## 2. Experimental methods

The compositions of the studied samples were $[(ZrO_2)_{0.92}(Y_2O_3)_{0.08}]_{1-x}(TiO_2)_x$ with $x=0.00$, 0.05, 0.10, 0.15, 0.20, 0.25 and 0.30 mol (compositions in wt% are also listed in Table 1). Samples will be labelled 0Ti, 5Ti, 10Ti, 15Ti, 20Ti, 25Ti and 30Ti.

The samples were prepared by addition of $TiO_2$ (Merck, 808, Darmstadt, Germany) to commercially available YSZ powders containing 8 mol% of $Y_2O_3$ (yttria-stabilized zirconia, Tosoh, Tokyo, Japan). Both powders have average particle diameters of 0.4 μm, and a specific surface area of $7\pm2$ and $15\pm4$ $m^2/g$, respectively. The particle size distribution was determined with a laser diffraction analyser (Matersizer S, Malvern, Worcerstershire, United Kingdom), and the specific surface area was measured by the $N_2$ adsorption method (Monosorb Surface Area Analyser MS13, Quantachrome Co., FL, USA).

The powder mixtures were submitted to attrition milling for 2 h, sieved (63 μm) and calcined at 800 °C for 2 h and sieved again (63 μm). Finally, the powder was pressed isostatically at 200 MPa into bars which were cut to prepare discs for their characterization. The samples were sintered in air at 1500 °C for 2 h (heating and cooling rates of 5 °C/min) according to the dilatometric studies. One sample (15Ti) was treated at 1500 °C for 120 h and quenched in air (heating rate of 5 °C/min) for comparative purposes. Constant heating rate (CRH, heating and cooling rates of 5 °C/min) experiments up to 1550 °C were performed in a differential dilatometer with alumina rod (Adamel Lhomargy, DI24, Brie, France). Final densities were measured by the Archimedes' immersion method in water. After sintering, the samples were weighted and treated in air, at 1500 °C, and then weighted again in order to evaluate the level of $Ti^{4+}$ reduction. In another set of experiments, the samples after sintering were weighted and treated at reducing atmosphere, at 1000 °C, and then weighted again to check the level of $Ti^{4+}$ reduction. X-Ray diffraction patterns of the samples were obtained using a Siemens D-5000 Diffractometer and monochromated high intensity Cu$K\alpha$ radiation and using Si as internal standard. The experimental diffraction patterns were collected at room temperature over a range of $20^\circ \le 2\theta \le 80^\circ$ (step-scanned at 1°/5 s). The XRD patterns obtained were analyzed using the diffraction files of $Zr_{0.92}Y_{0.08}O_{1.96}$ (JCPDS 01-82-1246), $Zr_{0.963}Y_{0.037}O_{1.982}$ (JCPDS 83-113), $Y_2Ti_2O_7$ (JCPDS 01-071-2065), $ZrTiO_4$ (JCPDS 34-415), $Zr_5Ti_7O_{24}$ (JCPDS 34-209), and Si (JCPDS 77-2111).

The phase distributions (in mol fraction) in the sintered materials were determined by the ratio [18]

$$M_c/M_t = 0.88[I_c(400)/I_t(400)+I_t(004)] \quad (1)$$

The experimental diffraction patterns for the phase distribution calculations were collected at room temperature over a range of $71^\circ \le 2\theta \le 75^\circ$ (step-scanned at 0.025°/20 s).

**Table 1**
Compositions considered in this work.

| Compositions (wt%) | Compositions (mol) | Label |
|---|---|---|
| $(ZrO_2)_{0.86}(Y_2O_3)_{0.14}(TiO_2)_{0.00}$ | $[(ZrO_2)_{0.92}(Y_2O_3)_{0.08}]_{1.00}(TiO_2)_{0.00}$ | 0Ti |
| $(ZrO_2)_{0.84}(Y_2O_3)_{0.13}(TiO_2)_{0.03}$ | $[(ZrO_2)_{0.92}(Y_2O_3)_{0.08}]_{0.95}(TiO_2)_{0.05}$ | 5Ti |
| $(ZrO_2)_{0.81}(Y_2O_3)_{0.13}(TiO_2)_{0.06}$ | $[(ZrO_2)_{0.92}(Y_2O_3)_{0.08}]_{0.90}(TiO_2)_{0.10}$ | 10Ti |
| $(ZrO_2)_{0.78}(Y_2O_3)_{0.12}(TiO_2)_{0.10}$ | $[(ZrO_2)_{0.92}(Y_2O_3)_{0.08}]_{0.85}(TiO_2)_{0.15}$ | 15Ti |
| $(ZrO_2)_{0.75}(Y_2O_3)_{0.12}(TiO_2)_{0.13}$ | $[(ZrO_2)_{0.92}(Y_2O_3)_{0.08}]_{0.80}(TiO_2)_{0.20}$ | 20Ti |
| $(ZrO_2)_{0.72}(Y_2O_3)_{0.11}(TiO_2)_{0.17}$ | $[(ZrO_2)_{0.92}(Y_2O_3)_{0.08}]_{0.75}(TiO_2)_{0.25}$ | 25Ti |
| $(ZrO_2)_{0.68}(Y_2O_3)_{0.11}(TiO_2)_{0.21}$ | $[(ZrO_2)_{0.92}(Y_2O_3)_{0.08}]_{0.70}(TiO_2)_{0.30}$ | 30Ti |

Furthermore, phase identification was also performed by FT-Raman spectroscopy using a Bruker FT 100/S spectrometer (Karlsruhe, Germany) with the YAG:Nd laser excitation (1064 nm) and a spectral resolution of 2 $cm^{-1}$.

The microstructure of the sintered samples was analyzed on polished (down to 1 μm) and thermally etched surfaces (1470 °C for 6 min, heating and cooling rates of 10 °C/min) by means of Field-emission scanning electron microscopy-energy dispersive X-ray (FE-SEM-EDX) (Hitachi S-4700 type I, Tokyo, Japan).

Samples prepared as pellets of 0.8 cm diameter and 0.2 cm thickness, were electroded with platinum high conductivity paste on both sample surfaces. Electrochemical impedance spectroscopy analyses (EIS) in air and under reducing atmosphere, between 250 and 1000 °C, by using a computer-assisted emf readings during the reduction and/or oxidation of the furnace atmosphere were performed. The impedance analyzer used was a HP 4192A (Palo Alto, CA, USA) in the frequency range of 10–$10^7$ Hz.

Impedance spectroscopy measurements at constant frequency (10 kHz) in a controlled-atmosphere furnace as a function of temperature (800–1000 °C) were also performed. The atmosphere was fitted with a YSZ oxygen sensor to ensure continuous monitoring of the oxygen partial pressure next to the pellet being characterized. The furnace atmosphere can be brought quickly from air to reducing conditions by a single flushing of the closed furnace chamber with a $N_2+H_2$ gas mixture. Data can be obtained while reducing or raising the $pO_2$ of the furnace atmosphere. The latter is usually preferred and it corresponds to a slow transition in $pO_2$ due to the permeation of oxygen through the sensor tube (electrochemical) and other possible minor physical leaks in the system.

## 3. Results and discussion

### 3.1. X-ray diffraction

Fig. 1 shows the XRD patterns of (a) 0Ti, (b) 5Ti and (c) 10Ti samples after sintering at 1500 °C for 2 h. The XRD pattern of the undoped sample matched with the diffraction file for the cubic zirconia $Zr_{0.92}Y_{0.08}O_{1.96}$ (JCPDS 01-82-1246). However, with titania additions the peaks are shifted to lower *d*-values with respect to the undoped sample and with respect to the diffraction file mentioned above. This behaviour may indicate the existence of a Ti-doped YSZ solid solution since the shift may be caused by replacement of the $Zr^{4+}$ ions (radius $Zr^{4+}$(VIII)=0.084 nm) by smaller $Ti^{4+}$ ions (radius $Ti^{4+}$(VIII)=0.074 nm) [19].

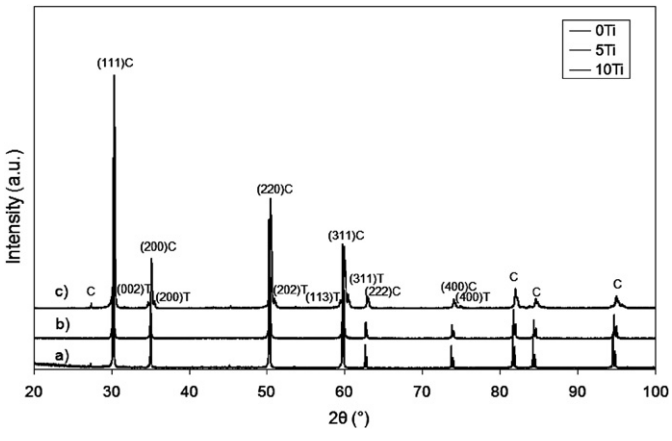


**Fig. 1.** XRD patterns of (a) 0Ti, (b) 5Ti and (c) 10Ti sintered at 1500 °C for 2 h. In (a) only the fluorite phase is detected. The presence of a tetragonal phase can be already noticed in (b) (5Ti) and more clearly in (c) (10Ti). The phases are labelled as C (YSZ or Ti-doped YSZ) and T (Ti-doped YTZP).

For the 5Ti sample not only a titania-doped YSZ solid solution is detected but also small peaks appear, which may be attributed to the formation of a tetragonal zirconia phase. It is well-known that in the cubic zirconia the coordination of $Zr^{4+}$ is 8 (equal distances), whereas in the tetragonal lattice the distances are not the same (6+2) [20]. Thus, the latter coordination is closer to that present in the rutile-type structure, where the $Ti^{4+}$ is six coordinated. Therefore, this fact could be the reason why the titanium addition leads to the formation of tetragonal zirconia.

For the 10Ti sample besides of the high intensity peaks corresponding to a titania-doped YSZ solid solution, peaks corresponding to a tetragonal zirconia phase becomes very clearly observed. The peaks that correspond to the cubic phase are further shifted towards lower *d*-values. The peaks that correspond to the tetragonal phase are also shifted with respect to the tetragonal zirconia pattern, i.e., $Zr_{0.963}Y_{0.037}O_{1.982}$ (JCPDS 83-113). For the latter phase, the diffraction peaks with Miller indices (*h* 0 0) show a shift to lower *d*-values whereas the (0 0 l) peaks are shifted to higher *d*-values. In addition, for the 15Ti sample besides of the two zirconia solid solutions an additional impurity phase can be detected (Fig. 2). This phase could be attributed to the pyrochlore-type structure with formula $Y_2Ti_2O_7$ (JCPDS 01-071-2065). However, the corresponding reflections are shifted with respect to the $Y_2Ti_2O_7$ pattern and this shift can be most likely attributed to the formation of a solid solution in which $Zr^{4+}$ ions can replace to $Ti^{4+}$ ions giving rise to $Y_2(Ti_{1-y},Zr_y)_2O_7$. The formation of the pyrochlore phase can be explained due to the extremely low Gibbs free energy formation: −4593 kJ/mol at 1000 °C and −4918 kJ/mol at 1500 °C, using the function given by Schaedler et al. [17].

When the concentration of $TiO_2$ reaches 20 mol%, $ZrTiO_4$ phase crystallizes and the concentration of this phase increases further with increasing $TiO_2$ content, as evidenced by increased intensity of the peaks characteristic for this phase (25Ti, Fig. 2). In addition, the reflections are shifted with respect to the $ZrTiO_4$ pattern (JCPDS 34-415), which can be due to the formation of a solid solution in which $Y^{3+}$ ions can replace $Ti^{4+}$. According to the calculations by Hom et al. [21] the formation of the titanate from the oxides is thermodynamically favourable from about 980 °C (1250 ± 150 K). However, it has been only reported up to now at temperatures between 1300 and 1600 °C [21–26]. In this work, the formation of zirconium titanate for samples with 20 mol% of titania or higher is observed from 1200 °C by XRD studies, although there must be taken into account that the precursors are 8YSZ and $TiO_2$ and they were, after mixing, calcined at 800 °C for 2 h previous to their sintering. According to Schaedler et al. [17] zirconium titanate has a Gibbs free energy at 1500 °C of −4918 kJ/mol. However, the exact composition of the titanate is still controversial. According to McHale and Roth [22] the stoichiometric zirconium titanate ($ZrTiO_4$) is the stable phase at high temperature (>1200 °C), whereas, for lower temperatures (<1100 °C) the composition of zirconium titanate shifts towards higher $TiO_2$ contents. For instance, those authors [22], after annealing compacts with the stoichiometric composition ($ZrTiO_4$) at 1000 °C for more than 4 months concluded that the composition of the stable phase of zirconium titanate below 1100 °C was $Zr_5Ti_7O_{24}$ [22]. For relatively short thermal treatments such as those used in ceramic processing, $Zr_5Ti_7O_{24}$ can be only formed in the presence of additives such as $Y_2O_3$ [24]. In our case, $Zr(Ti,Y)O_4$ will be formed at 1500 °C but part of it could transform to $Zr_5(Ti,Y)_7O_{24}$ during cooling down. However, by XRD the latter phase is not detected and according to EDX analyses (see below) on several grains of the zirconium titanate phase, a Zr/Ti atomic ratio between 0.8 and 1.2 was obtained, depending on the sample composition.

For 30Ti sample a similar XRD pattern than that of 25Ti is observed, although the peaks corresponding to the tetragonal phase are weaker.

XRD quantitative analyses were performed for the 10Ti and 15Ti samples. For these analyses according to Eq. (1), the pyrochlore phase which is an impurity phase has not been considered. The analyses for the 10Ti sample gave 0.68 mol fraction of titania-doped YSZ solid solution and 0.32 mol fraction of the tetragonal solid solution. The concentration of the tetragonal solid solution increases with increasing $TiO_2$ dopant level, i.e. the mol fraction of Ti-YTZP is 0.51 and of the cubic phase is 0.49 for 15Ti sample. Thus, it is a duplex material.

Weight measurements indicate that no significant weight loss was produced after the thermal treatment in air. In addition, XRD patterns after that treatment were similar to those after sintering.

### 3.2. FT-Raman studies

FT-Raman spectra of the samples considered in this study are presented in Fig. 3. The spectrum of 0Ti (YSZ) is dominated by the intense peak at 621 $cm^{-1}$ which is characteristic for the cubic phase of $ZrO_2$ [27]. Although only one Raman band is expected to be observed for the cubic phase (of $F_{2g}$ symmetry), the recorded spectrum shows also a number of weaker bands at about 690, 560, 496, 357, 235 and 152 $cm^{-1}$. Very similar results were reported in

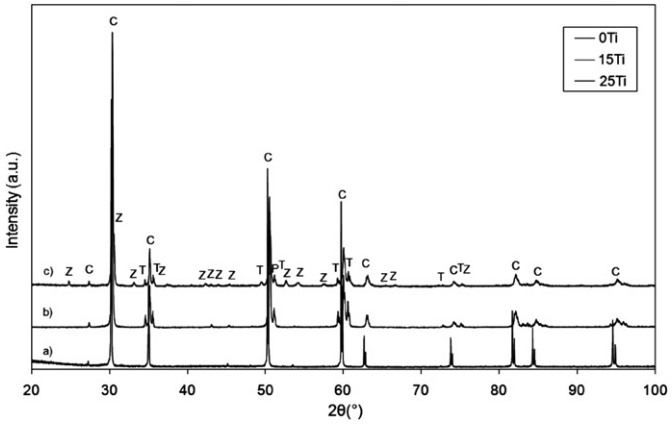


**Fig. 2.** XRD patterns of (a) 0Ti, (b) 15Ti and (c) 25Ti sintered at 1500 °C for 2 h. In (a) only the fluorite phase is detected. The presence of a tetragonal phase can be noticed in (b) (15Ti), while the formation of zirconium titanate is observed in (c). In 15Ti pyrochlore phase, as impurity phase, is also detected. The phases are labelled as C (YSZ or Ti-doped YSZ), T (Ti-doped YTZP), Z (zirconium titanate) and P (pyrochlore).

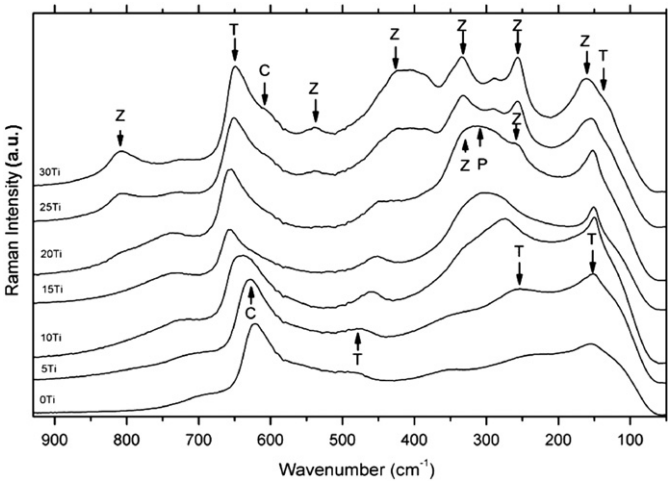


**Fig. 3.** FT-Raman spectra of YSZ doped with various amounts of $TiO_2$. The characteristic peaks for cubic zirconia, tetragonal zirconia, disordered pyrochlore and $ZrTiO_4$ phases are indicated by letters C, T, P and Z, respectively.

the literature for $Zr_{0.82}Y_{0.18}O_{1.91}$ [27,28]. These additional bands arise from local disorder introduced by $Y^{3+}$ ions.

In a similar way, the spectrum of the 5Ti sample is dominated by the intense peak at 628 $cm^{-1}$, which is characteristic for the cubic phase of $ZrO_2$ as was mentioned above [27,28]. Except for the 628 $cm^{-1}$ band, a few weak bands are observed at 702, 474, 355, 252 and 152 $cm^{-1}$. The 702 and 355 $cm^{-1}$ bands arise most likely from local disorder introduced by $Y^{3+}$ ions. The remaining bands have similar wavenumbers as bands of the tetragonal $ZrO_2$, which are observed at 151, 260 and 468 $cm^{-1}$ [29]. This result suggests that the 5Ti sample contains also a small admixture of the tetragonal phase, according to the XRD pattern. For the 10Ti sample, the bands of tetragonal and cubic zirconia solid solutions are also present. Furthermore, a band at 310 $cm^{-1}$ appears, which can be most likely attributed to a disordered pyrochlore phase [28]. The spectrum of the 15Ti sample differs significantly from the spectrum of pure YSZ (0Ti). First, the band near 621 $cm^{-1}$, characteristic for the cubic phase of $ZrO_2$, becomes much weaker. This result proves that the sample still contains cubic $ZrO_2$ but other phases are also present. Second, a very broad and intense band appears near 299 $cm^{-1}$ and also another broad band appears near 745 $cm^{-1}$. These broad bands are characteristic for a disordered pyrochlore phase [28]. Literature data show that the strongest band for $Y_2Ti_2O_7$ is observed near 309 $cm^{-1}$ but three other bands are also very clearly seen at 609, 522 and 448 $cm^{-1}$ [28]. When $Zr^{4+}$ ions are partially substituted for $Ti^{4+}$ ions, Raman bands become broader and a new, very broad band appears above 700 $cm^{-1}$ [28]. Moreover, the intensity of the 522 and 448 $cm^{-1}$ bands decreases with increasing concentration of the $Zr^{4+}$ ions and these bands disappear for $Y_2Ti_{0.6}Zr_{1.4}O_7$ [28]. Another characteristic feature is the appearance of a new and broad band near 150 $cm^{-1}$ for $Y_2Ti_{0.6}Zr_{1.4}O_7$, which is absent for smaller concentrations of $Zr^{4+}$ [28]. Although our spectrum shows a band near 152 $cm^{-1}$, which could indicate that concentration of the $Zr^{4+}$ ions in $Y_2(Ti_{1-y}Zr_y)_2O_7$ is much higher than that of $Ti^{4+}$, the bandwidth of this band is much smaller than that observed for $Y_2Ti_{0.6}Zr_{1.4}O_7$. Moreover, the shapes and intensities of the 299 and 745 $cm^{-1}$ bands are very similar to those reported in the literature for $Y_2Ti_{1.1}Zr_{0.9}O_7$ [28]. Our results give, therefore, strong evidence that the studied sample contains the $Y_2(Ti_{1-y}Zr_y)_2O_7$ pyrochlore phase with $y$ close to 1 or slightly higher than 1 (Fig. 3). In addition, two bands are observed at 657 and 454 $cm^{-1}$. These bands, together with the narrow band at 152 $cm^{-1}$, can be assigned to the tetragonal phase of $ZrO_2$ [27]. It is worthy to add that the tetragonal $ZrO_2$ should also show the presence of a relatively strong Raman band near 257 $cm^{-1}$ and two weak bands near 305 and 410 $cm^{-1}$ [27]. These bands are hidden in the broad envelope of the 299 $cm^{-1}$ band. In summary, our results show that for the 15Ti sample three phases are present: titania doped YSZ and titania doped YTZP solid solutions and, a disordered pyrochlore with formula $Y_2(Ti_{2-y}Zr_y)_2O_7$ ($y$ being close to 1 or slightly higher than 1) (Fig. 3). According to Zhu et al. [30] the formation of the pyrochlore phase can be explained to be the result of Y segregation and subsequent cation ordering in the fluorite structure. Pyrochlore, $A_2^{3+}B_2^{4+}O_7$, is a derivative of the fluorite structure, but with one-eighth fewer anions and two types of cation sites. The presence of the pyrochlore phase can be explained considering the short soaking time of the thermal treatment employed in this work (2 h) since it is a metastable phase [17].

When the concentration of $TiO_2$ increases further, significant changes occur in the spectra. First, the band near 628 $cm^{-1}$ shifts towards higher wavenumbers (656 $cm^{-1}$ for the 20Ti sample, see Table 2) and then again slightly towards lower wavenumbers (to 648 $cm^{-1}$ for the 30Ti sample). Moreover, a weak band near 620 $cm^{-1}$ becomes visible when the concentration of $TiO_2$ is 20 mol% or higher. Since the zirconia tetragonal phase should show a band near 643 $cm^{-1}$ [29], the observed changes in the Raman spectra can be attributed to a significant concentration increase of the tetragonal zirconia solid solution at the expense of the cubic one. Second, a new band appears near 794 $cm^{-1}$ for the 20Ti sample and it exhibits significant shift towards higher wavenumbers and large intensity increase with increasing concentration of $TiO_2$ (see Fig. 3 and Table 2). Since this band is characteristic for $ZrTiO_4$ [31] it is obvious from the Raman spectra that with the increasing concentration of $TiO_2$, the amount of $ZrTiO_4$ in the samples also increases. This conclusion is further supported by a strong intensity increase of the broad band near 422–385 $cm^{-1}$, which can be attributed to $ZrTiO_4$. The observed dependence of the ~800 $cm^{-1}$ band position on $TiO_2$ concentration suggests that there is not a pure phase of $ZrTiO_4$ but rather a solid solution of $ZrTiO_4$ and $Y_2O_3$ (Fig. 3).

Another characteristic feature of the Raman spectra is the appearance of new bands near 160, 260 and 334 $cm^{-1}$ when the concentration of $TiO_2$ is 20 mol% or higher. The intensities of these bands increase with increasing concentration of $TiO_2$. According to the literature data, strong bands are expected near 154–160 and 258–276 $cm^{-1}$ for $ZrTiO_4$ [31]. Moreover, a medium intensity band should appear for $ZrTiO_4$ near 327–333 $cm^{-1}$ [31]. A strong band at 249–257 $cm^{-1}$, as well as medium intensity bands at 148–155 and near 328 $cm^{-1}$, are also expected for tetragonal zirconia [27,29]. Since there is a clear correlation between intensities of the 160, 260 and 334 $cm^{-1}$ bands and intensities of the 806 and 422–389 $cm^{-1}$ bands characteristic for $ZrTiO_4$, we assign these bands to the presence of $ZrTiO_4$ phase.

Raman spectra of the 25Ti and 30Ti samples show also the presence of a weak band near 537 $cm^{-1}$. This band can also be attributed to $ZrTiO_4$ since the former studies reported in the

**Table 2**
Raman wavenumbers for YSZ doped with various amounts of $TiO_2$.

| 0Ti | 5Ti | 10Ti | 15Ti | 20Ti | 25Ti | 30Ti | Phase |
|---|---|---|---|---|---|---|---|
| | | | | 794w | 805w | 807m | $ZrTiO_4$ |
| 689w | 702w | 715w | 734w | 734w | 724w | 720w | Pyrochlore |
| | | 638s | 657s | 656s | 650s | 648s | Tetragonal $ZrO_2$ |
| 622s | 628s | 627m | 627m | 626w | 624w | 620w | Cubic $ZrO_2$ |
| | | | | | 537w | 539w | $ZrTiO_4$ |
| 487w | 474w | 458w | 455w | 448w | | | Tetragonal $ZrO_2$ |
| | | | | 399w | 405m | 405s | $ZrTiO_4$ |
| 355w | 340w | 334w | 330w | 330w | 332m | 334m | Tetragonal $ZrO_2$ and $ZrTiO_4$ |
| | | 310m | 305m | 310m | | | Pyrochlore |
| | | | | | 289w | 288w | ? |
| 242m | 252m | 274m | 278w | | | | Tetragonal $ZrO_2$ |
| | | | | 262w | 257m | 256m | $ZrTiO_4$ |
| | | | | | 157m | 160s | $ZrTiO_4$ |
| 152m | 152m | 152m | 152m | 152m | | 150m | Tetragonal $ZrO_2$ |

literature showed the presence of a weak Raman band near 537 $cm^{-1}$ for this compound. The 20Ti sample shows the presence of a broad band near 310 $cm^{-1}$, overlapped with the bands near 260 and 334 $cm^{-1}$. That band is characteristic for the $Y_2(Ti_{1-y}Zr_y)_2O_7$ pyrochlore phase. When the concentration of $TiO_2$ increases further, this band is not clearly observed since it is most likely overlapped by much stronger bands corresponding to $ZrTiO_4$.

Considering the heights of the small peaks relative to the pyrochlore XRD reflections, it is assumed that this phase separation is revealed by the crystalline segregations on the surface of the cubic grains and along the grain boundaries, as shown in Fig. 5(a) and (b) (see discussion in the next section). According to López-López et al. [32] in zirconium titanate based materials containing cubic zirconia, the pyrochlore phase is metastable and is formed during the heating treatment up to 1500 °C. Those authors explained this fact by the extremely low Gibbs free formation energy of pyrochlore, as was mentioned above, −4593 kJ/mol at 1000 °C or −4918 kJ/mol at 1500 °C using the function given by Schaedler et al. [17] Furthermore, according to Fagg et al. [33] fast cooling contributes to the prevention of ordering in the cation lattice and thus to the formation of the pyrochlore phase. In this study, the samples were sintered at 1500 °C for 2 h followed by cooling to room temperature at 5 °C/min, thus the formation of pyrochlore can be produced. When the 15Ti sample was treated at 1500 °C for 120 h and quenched in air for comparative purposes pyrochlore phase was not observed. This fact supports the observations of Fagg et al. [33]. Thus, longer sintering times [17] and fast cooling treatments [33] can avoid the formation of the pyrochlore phase.

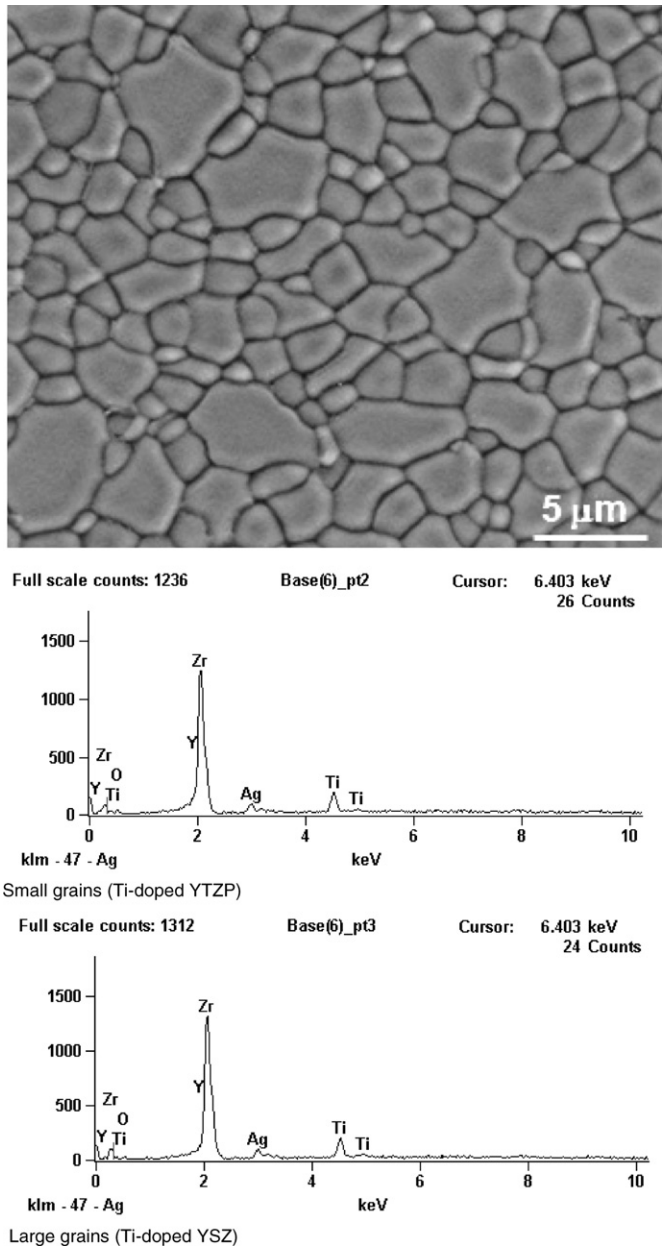


**Fig. 4.** FE-SEM micrograph of a polished and thermal etched surface, together with characteristic EDX analyses for 15Ti (duplex material).

### 3.3. FE-SEM-EDX studies

A typical microstructure of the 15Ti composite material sintered in air at 1500 °C for 2 h, after polishing and thermal etching, is shown in Fig. 4. Fully densified bodies were obtained for the 15Ti sample in comparison with undoped YSZ, which exhibited inter and intragranular porosities (not shown here). A bimodal grain size distribution is observed for the composite. Semiquantitative analyses gave ≈71–76 wt% $ZrO_2$, 12–19 wt% $Y_2O_3$, 9–11 wt% $TiO_2$, values for the large grains that can be identified with titania-doped YSZ solid solution, meanwhile the analysis gave ≈80–81 wt% $ZrO_2$, 5–7 wt% $Y_2O_3$, 11–12 wt% $TiO_2$, values for the small grains that should correspond to titania-doped YTZP. In addition, small crystalline segregations along the grain boundaries, and on the surface of the cubic grains (large grains) are detected when the samples are

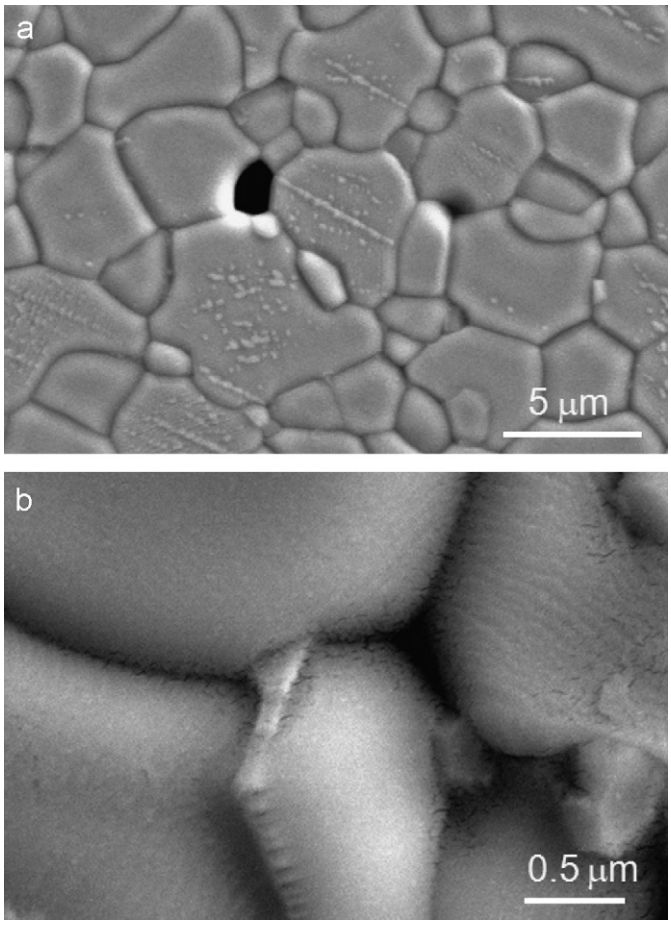


**Fig. 5.** FE-SEM micrographs of polished and thermal etched surfaces for the sample 15Ti (duplex material) where the pyrochlore segregation can be observed on the surface of the cubic grains (large grains) (a), and along the grains (b).

observed at higher magnifications (see Fig. 5(a) and (b)), which according to the Raman studies discussed above, can be attributed to the pyrochlore phase. Tietz et al. [34] also detected a pyrochlore segregation for samples with higher yttria content and the same titania content, 15 mol%, than in this study. However, they observed the pyrochlore phase at lower sintering temperatures (from 1200 to 1400 °C). Nevertheless, neither heating nor cooling rates were indicated in their study.

FE-SEM-EDX results for samples with a higher titania content are shown in Fig. 6. For the 25Ti sample semiquantitative analysis gave ≈75–67 wt% $ZrO_2$, 23–20 wt% $Y_2O_3$ and 12–10 wt% $TiO_2$ values for the large grains that can be identified with titania-doped YSZ solid solution. For smaller grains of the same tone the semiquantitaive analysis gave ≈76–81 wt% $ZrO_2$, 6–9 wt% $Y_2O_3$ and 13–12 wt% $TiO_2$, that can be identified with titania-doped YTZP. For the darker grains the analyses gave ≈63–67 wt% $ZrO_2$, 2–6 wt% $Y_2O_3$ and 33–43 wt% $TiO_2$ that can be identified as zirconium titanate in which yttrium oxide is in solid solution. For the 30Ti sample semiquantitative analysis gave ≈68–70 wt% $ZrO_2$, 18–20 wt% $Y_2O_3$ and 10–11 wt% $TiO_2$ values for the large and clear grey grains that can be identified with titania-doped YSZ solid solution, whereas the analysis gave ≈56–61 wt% $ZrO_2$, 2–6 wt% $Y_2O_3$ and 30–40 wt% $TiO_2$ values for the dark grey grains that could correspond to zirconium titanate. For this sample tetragonal grains were not analysed since their size is very small and an accurate analysis is not possible.

In summary, according to the results obtained by XRD, FT-Raman and FE-SEM-EDX it is clear that the titania enhances first the formation of a titania-doped YSZ solid solution, and second induces the formation of a titania-doped YTZP solid solution. According to XRD analyses the amount of the latter solid solution increases with increasing the addition of $TiO_2$ from 5 to 15 mol%. The $Y_2(Ti_{1-y}Zr_y)_2O_7$ pyrochlore phase is detected already for 5 mol% by FT-Raman. When the concentration of $TiO_2$ reaches about 20 mol%, zirconium titanate that admits $Y_2O_3$ in solid solution crystallizes and the concentration of this phase increases further with increasing $TiO_2$ content.

### 3.4. AC electrical measurements: impedance spectroscopy measurements in air

Fig. 7 presents the bulk ionic conductivity with the reciprocal of the temperature for the YSZ (0Ti), the YTZP and 0.51 mol fraction Ti-YTZP/0.49 mol fraction Ti-YSZ (15Ti) compositions. The ionic conductivity is lower for the composite material, i.e., an increase in bulk resistance of the material is observed, which corresponds to an overall conductivity drop of about 6 times when compared to 8YSZ (Fig. 7). As titanium is a tetravalent dopant, the concentration of oxygen vacancies is determined by the concentration of yttrium, which means that only a slight overall decrease in concentration of ionic defects should be noticed between undoped (0Ti) and doped material (15Ti), as a consequence of a simple dilution effect, if both samples were constituted by cubic phase. Therefore, dilution effect due to the

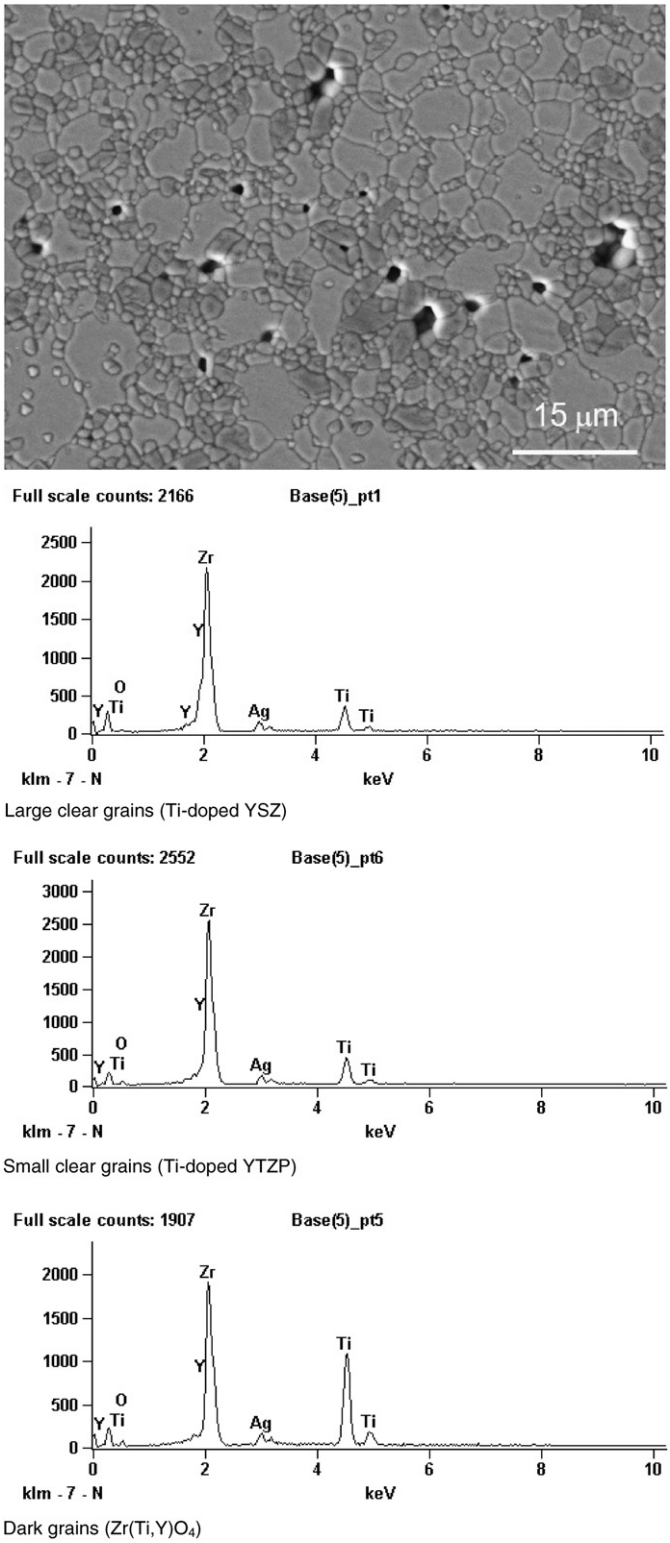


**Fig. 6.** FE-SEM micrograph of polished and thermal etched surface, together with characteristic EDX analyses for 25Ti.

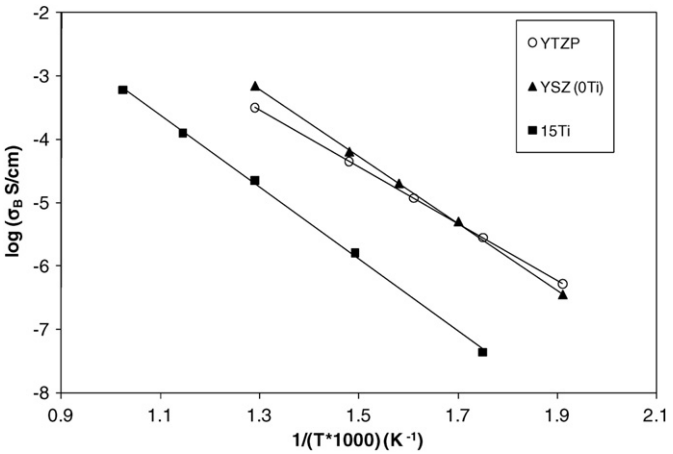


**Fig. 7.** Log bulk conductivity of YSZ, YTZP, and 15Ti in air as a function of the reciprocal of the temperature.

substitution of $Zr^{4+}$ by $Ti^{4+}$ plays a negligible role in the bulk resistivity reduction. In addition, to consider the role of dopants on the conductivity, it is important to take into consideration the effective pathway for oxygen ions moving between adjacent sites, that promotes the free radius effect. Based on the ionic radius of $Zr^{4+}$ (VIII)=0.084 nm and $Ti^{4+}$ (VIII)=0.074 nm [19], it can be concluded that the substitution of $Zr^{4+}$ by $Ti^{4+}$ causes an increment in the free radius. This is expected to yield an increase in ionic conductivity and a decrease in the activation energy for ionic mobility. However, the present results do not agree with the effective pathway model. Therefore, we conclude that in the present case the simple effect of the dopant cation radius is not responsible for the resistivity enhancement. If the temperature range between 350 and 500 °C is considered, the values of the bulk activation energy are $1.00 \pm 0.02$ eV for 0Ti (8YSZ), $0.89 \pm 0.03$ eV for YTZP, and $1.08 \pm 0.03$ eV for 15Ti (Fig. 7). Thus, the activation energy for ionic migration in 15Ti is similar to that of 8YSZ (0Ti), i.e., the process is controlled by the oxygen vacancies migration in titania-doped YSZ grains with the highest value of activation energy. In addition, the effect of dopant level on the energy value is negligible. Therefore, we conclude that the high decrease of the ionic conductivity is observed since the sample is composed of tetragonal and cubic domains having different conductivities, mainly because of the lower oxygen vacancy content in the tetragonal grains. There must be also taken into account the effect of the pyrochlore phase on the bulk ionic conductivity. The formation of the $Y_2(Ti_{1-y}Zr_y)_2O_7$ pyrochlore phase may change the composition of the cubic grains. According to Fagg et al. [33] the presence of $Y_2Ti_2O_7$ increases the bulk ionic conductivity of $Y_{0.2}Ti_{0.18}Zr_{0.62}O_{1.9}$ cubic sample, since the Zr/Y and the Zr/Ti ratios increase with increasing quantities of the $Y_2Ti_2O_7$. In our case, the effect of the pyrochlore formation on both ratios should be quantified in order to establish their influence on the bulk ionic conductivity of the cubic grains.

### 3.5. Dependence of electrical conductivity on $pO_2$

For this study, the sample with 15Ti has been selected since this composition may have a sufficient electronic conductivity as matrix for a SOFC anode. Weight measurements indicated a weight loss of sintered samples after treatment with a reducing gas mixture. It is assumed that this process involved both the formation of oxygen vacancies and a partial reduction of $Ti^{4+}$ ions to $Ti^{3+}$.

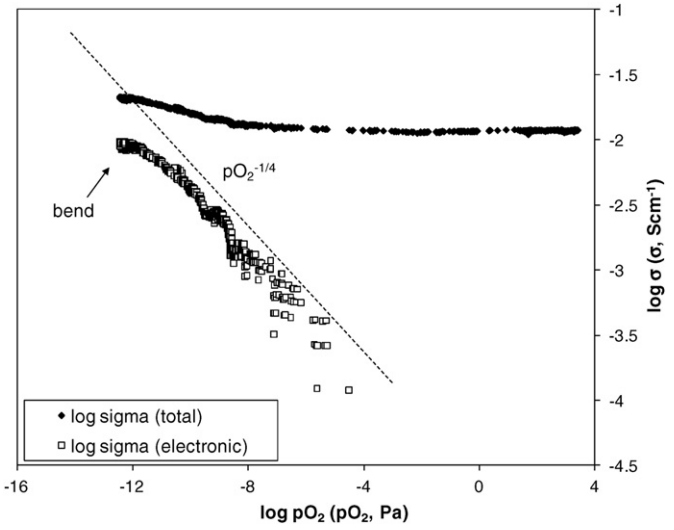


**Fig. 8.** Dependence of electrical conductivity (10 kHz) on oxygen partial pressure for 15Ti (duplex material) at 1000 °C.

Fig. 8 presents the dependence of the total ($\sigma_T$) and the electronic conductivity ($\sigma_e$) on oxygen partial pressure at 1000 °C for the 15Ti sample. In the $pO_2$ range from 0.21 to $10^{-7.5}$ atm, the conductivity is predominantly ionic and constant over the range and its value is 0.01 S/cm. The electronic contribution $\sigma_e$ has been calculated according to the equation $\sigma_e=\sigma_T-\sigma_i$, assuming that the concentration of oxygen vacancies is effectively constant over the investigated $pO_2$ range from 0.21 to $10^{-12.4}$ atm and that the value for $\sigma_T$ gives the value of the ionic conductivity $\sigma_i$ at high $pO_2$. The onset in the electronic conductivity under reducing conditions might exhibit a $-1/4$ or a $-1/6$ dependence [6,35]. The first result should be expected for the increase in electronic defects associated with the reduction of titanium ions in the cation sublattice:

$$O_o + 2Ti_{Zr}^{x} = V_{\ddot{O}} + 2Ti_{Zr}^{\prime} + \tfrac{1}{2}O_2 \quad (2)$$

In this reaction it has been assumed the Kröger–Vink type of notation for defects. In particular, the symbol $Ti_{Zr}^{\prime}$ corresponds to one electronic defect localized in a titanium ion in the cation sublattice (small polaron), or in other words to a $Ti^{4+}$ plus trapped electron = $Ti^{3+}$ on Zr sites. In addition, $Ti_{Zr}^{x}$ represents a $Ti^{4+}$ ion on a Zr site. Applying the law of mass action the following equation can be obtained:

$$K = [Ti_{Zr}^{\prime}]^2[V_{\ddot{O}}]pO_2^{1/2} \quad (3)$$

Assuming that $[Ti_{Zr}^{x}]$ is constant, i.e., $[Ti_{Zr}^{x}] \gg [Ti_{Zr}^{\prime}]$, the electrical neutrality is given by

$$[Ti_{Zr}^{\prime}] + [Y_{Zr}^{\prime}] = 2[V_{\ddot{O}}] \quad (4)$$

From Eqs. (2) and (3) the dependence of oxygen partial pressure on $Ti^{3+}$ concentration can be expressed as follows: $[Ti_{Zr}^{\prime}] \propto pO_2^{-1/4}$.

Electronic conductivity is introduced into the system at oxygen partial pressures below $10^{-8.3}$ atm via reduction of $Ti^{4+}$ ions to $Ti^{3+}$. A bend has been observed at very low oxygen partial pressures ($pO_2 \sim 10^{-12}$ Pa) as was also observed by Kaiser et al. [36] for $Y_{0.2}Ti_{0.18}Zr_{0.62}O_{1.9}$, indicating that the reduction kinetics were too slow to achieve a complete reduction of the samples.

The calculated slope for this log ($\sigma_e$) vs. log ($pO_2$) plot follows a $pO_2^{-1/4}$ from $10^{-8.3}$ to $10^{-12.4}$ atm. The ionic plus electronic conductivity is 0.02 S/cm at 1000 °C and $10^{-12.3}$ atm. Therefore, it is concluded that the n-type electronic conduction in 15Ti constituted by 0.51 mol fraction of TiYTZP/0.49 mol fraction of TiYSZ can be due to a small polaron-hopping between $Ti^{3+}$ and $Ti^{4+}$ ions.

## 4. Conclusions

- It has been established that the duplex material constituted by 0.51 mol fraction TiYTZP/0.49 mol fraction TiYSZ is obtained by solid state reaction after an addition of 15 mol% $TiO_2$ to 8YSZ.
- From 5 mol% of $TiO_2$, $Y_2(Ti_{1-y},Zr_y)_2O_7$ pyrochlore is present as a minor phase, being $y$ close to 1 according to FT-Raman studies.
- For samples with $TiO_2$ contents from 20 mol%, zirconium titanate ($ZrTiO_4$) phase is detected apart of Ti-doped YTZP and Ti-doped YSZ solid solutions. Zirconium titanate admits $Y_2O_3$ in solid solution according to FE-SEM-EDX.
- It has been established that the duplex material studied in this work is a mixed conductor under low partial pressures and the onset of the electronic conductivity under reducing conditions exhibit a $-1/4$ $pO_2$ dependence.
- The ionic plus electronic conductivity for the duplex material is 0.02 S/cm at 1000 °C and $10^{-12.3}$ atm, being the n-type electronic conduction due to a small polaron-hopping between $Ti^{3+}$ and $Ti^{4+}$.

## Acknowledgments

The authors are grateful to Dr. D.P. Fagg for the electrical measurements under reducing atmosphere that he performed. This work has been supported by the Spanish Ministry of Science and Innovation (MAT2009-14369-C02-01).

## References

[1] E.J.L. Schouler, Solid State Ion. 9–10 (1983) 945.
[2] S.S. Liou, W.L. Worrell, Appl. Phys. A 49 (1) (1989) 25.
[3] R.M.C. Marques, J.R. Frade, F.M.B. Marques, in: G. Ziegler, H. Hausner (Eds.), Proceedings of the Euroceramics II, vol. 3, Deutsche Keramische Gesellschaft e.V., Augsburg, 1991, p. 2179.
[4] R.M.C. Marques, J.R. Frade, F.M.B. Marques, in: S.C. Singhal, H. Iwahara (Eds.), Proceedings of the Third International Symposium on Solid Oxide Fuel Cells, vol. 93–94, The Electrochemical Society Inc., Pennington, NJ, 1993, p. 513.
[5] M.T. Colomer, J.R. Jurado, R.M.C. Marques, F.M.B. Marques, in: S.C. Singhal, H. Iwahara (Eds.), Proceedings of the Third International Symposium on Solid Oxide Fuel Cells, vol. 93–94, The Electrochemical Society Inc., Pennington, NJ, 1993, p. 523.
[6] M.T. Colomer, R.M.C. Marques, J.R. Jurado, F.M.B. Marques, Mater. Res. Bull. 30 (4) (1995) 515.
[7] M.T. Colomer, P. Durán, A. Caballero, J.R. Jurado, Mater. Sci. Eng. A 229 (1–2) (1997) 114.
[8] M.T. Colomer, J.R. Jurado, J. Eur. Ceram. Soc. 19 (2) (1999) 143.
[9] M.T. Colomer, J.R. Jurado, J. Solid State Chem. 165 (1) (2002) 79.
[10] X. Mantzouris, N. Zouvelou, V.A.C. Haanappel, F. Tietz, P. Nikolopoulos, J. Mater. Sci. 42 (2007) 10152.
[11] B.J. Chen, Z.Q. Zeng, Key Eng. Mater. 336–338 (1–3) (2007) 2254.
[12] H. Miyazaki, Int. J. Appl. Ceram. Technol. 5 (5) (2008) 490.
[13] M. Gathee, J.T.S. Irvine, Int. J. Hydrogen Energy 35 (2010) 9427.
[14] N. Bonanos, R.K. Slotwinski, B.C.H. Steele, P. Butler, J. Mater. Sci. Lett. 3 (3) (1984) 245.
[15] R.P. Ingel, D. Lewis, B.A. Bender, R.W. Rice, J. Am. Ceram. Soc. 65 (9) (1982) C150–C152.
[16] A.J. Feighery, J.T.S. Irvine, D.P. Fagg, A. Kaiser, J. Solid State Chem. 143 (2) (1999) 273.
[17] T.A. Schaedler, O. Fabrichnaya, C.G. Levi, J. Eur. Ceram. Soc. 28 (13) (2009) 2509.
[18] R.A. Miller, J.L. Smialek, R.G. Garlick, in: A.H. Heuer, L.W. Hobbs (Eds.), Advances in Ceramics, vol. 3, American Ceramic Society, Columbus, OH, 1981, p. 241.
[19] R.D. Shannon, Acta Crystallogr. A 32 (1976) 751.
[20] L.S.M. Traqueia, T. Pagnier, F.M.B. Marques, J. Eur. Ceram. Soc. 17 (8) (1997) 1019.
[21] B.K. Hom, R. Stevens, B.F. Woodfield, J. Boeiro-Goates, L. Putnam, K.B. Helean, A. Navrotsky, J. Chem. Thermodyn. 33 (2) (2001) 165.
[22] A.E. McHale, R.S. Roth, J. Am. Ceram. Soc. 69 (1986) 827.
[23] R. Christoffersen, P.K. Davies, Solid State Ion. 57 (1–2) (1992) 59.
[24] F. Azough, A. Wrigth, R. Freer, J. Solid State Chem. 108 (1994) 284.
[25] N. Vittayakorn, J. Ceram. Process. Res. 7 (2006) 288.
[26] V. Licina, A. Gajovic, A. Mogus-Milankovic, I. Djerdj, N. Tomasic, D. Su, J. Am. Ceram. Soc. 91 (2008) 178.
[27] T. Hirata, E. Asari, M. Kitajima, J. Solid State Chem. 110 (1994) 201.
[28] M. Glerup, O.F. Nielsen, F.W. Poulsen, J. Solid State Chem. 160 (2001) 25.
[29] V. Lughi, D.R. Clarke, J. Appl. Phys. 101 (5) (2007) 053524.
[30] S. Zhu, X.T. Zu, L.M. Wang, R.C. Ewing, Appl. Phys. Lett. 80 (2002) 4327.
[31] F. Azough, R. Freer, J. Petzelt, J. Mater. Sci. 28 (1993) 2273.
[32] E. López-López, M.L. Sanjuán, R. Moreno, C. Baudín, J. Eur. Ceram. Soc. 29 (2009) 3219.
[33] D.P. Fagg, J.R. Frade, M. Mogensen, J.T.S. Irvine, J. Solid State Chem. 180 (2007) 2371.
[34] F. Tietz, W. Jungen, P. Lersch, M. Figaj, K.D. Becker, D. Skarmoutsos, Chem. Mater. 14 (5) (2002) 2252.
[35] H. Naito, H. Arashi, Solid State Ion. 53–56 (1992) 436.
[36] A. Kaiser, A.J. Feighery, D.P. Fagg, J.T.S. Irvine, Ionics 4 (1998) 225.